Supporting Information

Biosynthesis of *t*-Butyl in Apratoxin A: Functional Analysis and Architecture of a PKS Loading Module

Meredith A. Skiba[a,b*], Andrew P. Sikkema[a,b*], Nathan A. Moss[c], Andrew N. Lowell[a], Min Su[a], Rebecca M. Sturgis[a], Lena Gerwick[c], William H. Gerwick[c,d], David H. Sherman[a,e,f,g], Janet L. Smith[a,b]

[a]Life Sciences Institute, University of Michigan, Ann Arbor, MI 48109;
[b]Department of Biological Chemistry, University of Michigan, Ann Arbor MI, 48109;
[c]Center for Marine Biotechnology and Biomedicine, Scripps Institution of Oceanography, University of California, San Diego, La Jolla, CA 92093;
[d]Skaggs School of Pharmacy and Pharmaceutical Sciences, University of California, San Diego, La Jolla, CA 92093;
[e]Department of Medicinal Chemistry,
University of Michigan, Ann Arbor, MI 48109;
[f]Department of Chemistry, University of Michigan, Ann Arbor, MI 48109;
[g]Department of Microbiology and Immunology, University of Michigan, Ann Arbor, MI 48109

[*]These authors contributed equally to this work
To whom correspondence should be addressed JanetSmith@umich.edu

Supporting Methods

Culturing, extraction, and purification of apratoxin A

Culture conditions of *Moorea bouillonii* PNG 5-198 were identical for [methyl-^{13}C]methionine and labeled [1-^{13}C]propionate feeding experiments. Apratoxin A producer *M. bouillonii* PNG 5-198 was cultured in SW-BG11 media between 27-28°C, under light of 5.4-10.8 μmol photons m^{-2} S^{-1}. Two batches of 0.5 g wet filaments 1 cm in length were inoculated into 250 mL Erlenmeyer flasks and grown for 14 days, followed by sub-culturing of each biomass flask into two 2.8 L Fernbach flasks containing 1 L of media. After growth for ten days, the biomass from each flask was combined into one 2.8 L Fernbach flask containing 750 mL media, and the culture was equilibrated for an additional 7 days. [Methyl-^{13}C]methionine (Cambridge Isotopes) was added to the culture in three batches of 20 mg each over 13 days, to a final concentration of 0.53 mM, and harvested after an additional 6 days of growth. [1-^{13}C]propionate (Cambridge Isotopes) was added to a separate culture flask with a similar quantity of biomass in three batches of 28.8 mg over period of 15 days, to a final concentration of 1.2 mM, and harvested after an additional 15 days of growth. Cultures were harvested and lightly washed with DI water over a Büchner funnel with filter paper, followed by extraction with 2:1 CH_2Cl_2:MeOH. Crude extracts were fractionated by C18 SPE (Agilent) and eluted with 40%, 80%, and 100% acetonitrile, then 100% CH_2Cl_2. The 80% and 100% acetonitrile fractions were combined and further purified by HPLC using a gradient of 65% to 99% acetonitrile in H_2O + 0.1% formic acid at 3 mL min^{-1} through a 150 x 10 mm, 5 μM Kinetex C18 semi-preparative column. Subsequent semipure apratoxin A plus demethylated analogs were re-submitted for HPLC using a gradient of 70% to 81% acetonitrile in H_2O + 0.1% formic acid at 4 mL min^{-1}, rendering 1.2 mg of apratoxin A from the [1-^{13}C]propionate experiment and 1.8 mg of apratoxin A from the [methyl-^{13}C]methionine

experiment. Approximately 2 mg of apratoxin A harvested from previous non-labeled batches was similarly obtained and used for NMR enrichment comparisons.

NMR Analysis and Calculation of ^{13}C Incorporation Levels

All ^{13}C NMR analyses were performed on a Varian VX500 spectrometer at 500 MHz for ^{1}H NMR and 125 MHz for ^{13}C NMR. A JEOL ECZ500 spectrometer was used to obtain HSQC and HMBC spectra (data not shown) in order to confirm $^{13}C/^{1}H$ shifts of apratoxin A in D_4-methanol solvent used in the analysis of the [1-^{13}C]propionate feeding experiment (Supplementary Table 1). Residual solvent shifts in each sample were used as the chemical shift references. Sample processing was performed using MestReNova and Delta. Table 1 indicates ^{13}C-enrichment by carbon number in the [methyl-^{13}C]methionine feeding experiment, using a normalization method adapted from previous studies[1]. Briefly, integrated values of natural-abundance apratoxin A ^{13}C NMR signals are indicated in column 4. Five carbon atoms with different biosynthetic origins and chemical shifts were used for normalization between unenriched and enriched spectra: C7, C13, C20, C30, and C37. Normalization factors (columns 5-9) were obtained by dividing the integral values of all ^{13}C NMR signals in column 4 by those of C7, C13, C20, C30, and C37 (underlined in column 4). Then, the integral for the enriched signals of each of the five carbon atoms used in the normalization procedure (underlined in column 10) were multiplied by their normalization factors (columns 5-9) to obtain an expected signal integral for all carbon signals if no enrichment had occurred (columns 11-15). Percent enrichment was calculated by subtracting columns 11-15 from column 10, dividing the result by the column 11-15 values (*(enriched – expected unenriched)/expected unenriched*), and multiplying by 100 to yield the values in columns 16-20. The five results in columns 16-20 were averaged to yield the values in column

21. Column 22 is another expression of enrichment, namely the fold change of the enriched vs. unenriched sample.

Construct Design

All constructs for apratoxin biosynthetic proteins were amplified from a plasmid encoding full length *aprA* (pAPS1)[2] and inserted into pMCSG7[3] by ligation independent cloning (LIC) to create expression plasmids for AprA ΨGNAT-MT2 (residues 502-1022, pAPS4), AprA ΔACP (residues 2-1034, pAPS5), and AprA MT2 (residues 628-1022, pMAS247). Primers are listed in Supplementary Table 4. All *aprA* site-directed mutations were introduced into pMAS247 using the QuickChange protocol (Stratagene). Plasmid pMAS308 encoding BryX MT2 (residues 656-1052) was amplified from a *Candidatus Endobugula sertula* cosmid library[4] and inserted into pMCSG7 via LIC. DNAs encoding FabD and AprI ACP (residues 2085-2201) were amplified from *Moorea bouillonii* PNG 5-198 genomic DNA[5] and inserted into pMCSG7 via LIC to produce pMAS337 and pMAS373, respectively. All constructs and mutations were verified by Sanger sequencing at the University of Michigan DNA Sequencing Core.

Protein Expression and Purification

AprA apo-ACP and AprA MT1-ΨGNAT were expressed and purified as described previously[2]. In order to produce AprA holo-ACP and AprI holo-ACP, plasmids were transformed into *Escherichia coli* strain BAP1[6] and expressed and purified identically to AprA ACP. pAPS4 (AprA ΨGNAT-MT2), pMAS247 (AprA MT2), and pMAS337 (FabD) were transformed into *Escherichia coli* strain BL21(DE3), grown in 0.5 L of TB media with 100 μg mL^{-1} ampicillin to an OD_{600} = 1-2 at 37°C. Cultures were cooled to 20°C, induced with 200 μM IPTG, and

expressed overnight. To produce AprA ΔACP, pAPS5 was transformed into BL21(DE3) containing the pRare-CDF plasmid[7] and the pG-KJE8 plasmid (Takara) encoding the DnaK, DnaJ, GrpE, GroEL and GroES chaperones. Cells were grown in 0.5 L of TB media with 100 μg mL^{-1} ampicillin, 50 μg mL^{-1} spectinomycin, and 35 μg mL^{-1} chloramphenicol at 37°C. *dnaK*, *dnaJ*, and *grpE* were induced with 0.2 % (w/v) arabinose at OD_{600} = ~1. Cultures were grown for an additional 30 minutes at 37°C, cooled to 20°C for 1 hour, induced with 120 μM IPTG, and expressed overnight.

AprA MT2 and BryX MT2 cell pellets were resuspended in 35 mL Tris buffer A (50 mM Tris pH 7.4, 300 mM NaCl, 10% (v/v) glycerol, 20 mM imidazole) with 0.1 mg mL^{-1} lysozyme, 0.05 mg mL^{-1} DNase, and 2 mM $MgCl_2$, incubated on ice for 30 min, lysed by sonication, and cleared by centrifugation (38,650 x g, 30 min). Supernatant was filtered with a 0.45 μm syringe filter, loaded onto a 5 mL HisTrap column (GE Healthcare), washed with 10 column volumes of Tris buffer A, and eluted with a 5-100% linear gradient of Tris buffer B (50 mM Tris pH 7.4, 300 mM NaCl, 10% (v/v) glycerol, 400 mM imidazole). Proteins were further purified by size exclusion chromatography (HiLoad 16/60 Superdex S200) in Tris buffer C (50 mM Tris pH 7.4, 150 mM NaCl, 10% (v/v) glycerol).

FabD was purified identically to AprA MT2 and BryX MT2 with the addition of 100 mM urea to the lysis buffer. Following size-exclusion chromatography, FabD was diluted into Tris buffer D (50 mM Tris pH 7.4, 20 mM NaCl, 10% glycerol) and further purified by anion exchange. The protein was loaded onto a 5 mL HiTrap Q column (GE Healthcare), washed with 10 column volumes of Tris Buffer E (50 mM Tris pH 7.4, 10% glycerol), and eluted with a 0-100 % gradient of Tris buffer F (50 mM Tris pH 7.4, 1M NaCl, 10% glycerol) over 40 column volumes, and dialyzed overnight into Tris buffer C.

AprA ΨGNAT-MT2 cell pellets were resuspended in 5 mL Tris buffer G (100 mM Tris pH 7.9, 500 mM NaCl, 5% glycerol, 15 mM imidazole) / g of cell paste. Resuspended cell pellets were incubated on ice with 4 mg DNase, 10 mg lysozyme, and 4 mM $MgCl_2$ for 30 min. Cells were lysed by three passes through an Avestin EmulsiFlex-C3 homogenizer and clarified by centrifugation at 30,000 x g. The supernatant was loaded onto a 5mL HisTrap column and eluted with a 10-100% gradient of Tris buffer H (100 mM Tris pH 7.9, 500 mM NaCl, 5% glycerol, 300 mM imidazole). The His-tag was removed by overnight incubation with tobacco etch virus protease in Tris buffer I (50 mM Tris pH 7.9, 100 mM NaCl, 10% glycerol) followed by a second 5-mL HisTrap column. AprA ΨGNAT-MT2 was further purified via size exclusion chromatography (HiLoad 16/600 Superdex 200) in Tris buffer J (50 mM Tris pH 7.9, 100 mM NaCl).

AprA ΔACP cell pellets were resuspended in 5 mL HEPES buffer A (50 mM HEPES pH 7, 50 mM $(NH_4)_2SO_4$, 10 % glycerol, 15 mM imidazole) / g of cell paste. Resuspended cell pellets were incubated on ice with 4 mg DNase, 10 mg lysozyme, and 4 mM $MgCl_2$ for 30 min. Cells were lysed by three passes through an Avestin EmulsiFlex-C3 homogenizer and clarified by centrifugation at 30,000 x g. The supernatant was loaded onto a 5 mL HisTrap column and eluted with a 10-100% gradient of HEPES buffer B (50 mM HEPES pH 7, 50 mM $(NH_4)_2SO_4$, 10 % glycerol, 300 mM imidazole). AprA ΔACP was further purified via size exclusion chromatography (HiLoad 16/600 Superdex 200) in HEPES Buffer C (50 mM HEPES pH 7, 50 mM $(NH_4)_2SO_4$, 10 % glycerol). The sample was buffer exchanged into 50 mM HEPES pH 7, 100 mM NaCl via size exclusion chromatography (HiLoad 16/600 Superdex 200) prior to EM analysis.

Dimethylmalonyl-thiophenol synthesis

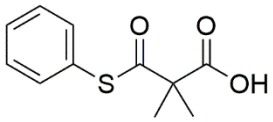

2,2-Dimethyl-3-oxo-3-(phenylthiol)propanoic acid. The following reaction was adapted from a published procedure[8]. Dimethyl malonic acid (1.36 g, 10.3 mmol) and thiophenol (1.06 mL, 10.3 mmol) were dissolved in acetonitrile (120 mL) and stirred in an ice bath. Diisopropylcarbodiimide (1.01 mL, 6.52 mmol) was slowly added and the mixture was warmed to room temperature overnight with stirring. The reaction was quenched by the addition of saturated sodium bicarbonate (500 mL), filtered, and extracted with Et_2O (2 x 250 mL). The aqueous layer was carefully acidified by the addition of 4 M HCl (pH = 2) and extracted with Et_2O (3 x 250 mL). The organic layers used to extract the acidic aqueous layer were combined, washed with brine (500 mL), dried with Na_2SO_4, and concentrated to a colorless oil. The oil was recrystallized from Et_2O/hexanes to give a mixture (0.329 g) of 2,2-dimethyl-3-oxo-3-(phenylthio)propanoic acid and diisopropyl urea as a white crystalline solid. The mother liquor was concentrated to a colorless oil and purified using a flash chromatography system (16-100% EtOAc/hexanes, SiliaSep HP 12 g, 36 mL min^{-1}) to give an amorphous white solid. This residue was purified using a flash chromatography system (16-25% EtOAc/hexanes, SiliaSep HP 12 g, 36 mL min^{-1}) to give 2,2-dimethyl-3-oxo-3-(phenylthio)propanoic acid (0.204 g, 13.9%) as an amorphous white powder: ^1H NMR (400 MHz, $CDCl_3$) δ 7.42 (s, 5H), 1.62 (s, 6H); ^{13}C NMR (100 MHz, $CDCl_3$) δ 198.5, 177.4, 135.0, 129.9, 129.5, 126.8, 57.3, 23.3; HRMS (ES) calcd for $C_{11}H_{12}O_3SNa$ (MNa^+) 247.0399, found 247.0397.

Production of acyl-ACPs

In order to produce malonyl- (Mal-), methylmalonyl- (MeMal-), and acetoacetyl- (AcAc-) ACP, 180 μM AprA apo-ACP was incubated with 20 μM *Streptomyces verticillus* phosphopantetheinyl transferase (SVP)[9], 20 mM $MgCl_2$, and 3-4 fold molar excess of the corresponding CoA for 4 hr at 30°C in Tris buffer C. Acyl-ACPs were purified from reaction mixtures using size exclusion chromatography (HiLoad 16/60 Superdex S75) equilibrated with 100 mM Tris pH 7.4, 250 mM NaCl, 5% glycerol, 5 mM Tris(2-carboxyethyl)phosphine hydrochloride (TCEP).

Dimethylmalonyl- (Me_2Mal-)ACP for intact protein spectra was prepared by incubating 300 μM AprA MeMal-ACP with 150 μM AprA MT1, 3 mM $(NH_4)_2Fe(SO_4)_2$, and 6 mM SAM in 50 mM HEPES pH 7.4, 150 mM NaCl. Reaction mixtures (500 μL) were incubated at 30°C for 5.5 hours. Me_2Mal-ACP was isolated from the reaction mixture via size exclusion chromatography (HiLoad 16/600 Superdex 75) with 100 mM Tris pH 7.4, 250 mM NaCl, 5% glycerol, 5 mM TCEP. Me_2Mal-ACP for Ppant ejection experiments was prepared by incubating 100 μM AprA holo-ACP with 25 mM Me_2Mal-thiophenol in 300 mM sodium bicarbonate pH 8.1 at 25°C overnight. Excess thiophenol was removed via size exclusion chromatography (HiLoad 16/600 Superdex 75) with 100 mM Tris pH 7.4, 250 mM NaCl, 5% glycerol, 5 mM TCEP.

AprA MT2 Enzyme Assays

Reaction mixtures (10 μL) containing 100 μM Me_2Mal-ACP, 25 μM AprA MT2, and 0.5 mM SAM, SAH, or sinefungin in 50 mM HEPES pH 7.4, 150 mM NaCl, 0.5 mM $MgCl_2$ were

incubated at 30°C for 1 min. Reactions were quenched with 10% (v/v) formic acid, and 0.25 μL of reaction mixtures were subjected to LC-MS analysis.

Reaction mixtures (10 μL) containing 100 μM MeMal-ACP, 25 μM AprA MT2, and 0.5 mM SAM, SAH, or sinefungin in 50 mM HEPES pH 7.4, 150 mM NaCl, 0.5 mM $MgCl_2$ were incubated at 30°C for 10 min. Reactions were quenched with 10% (v/v) formic acid, and 0.25 μL of reaction mixtures were subjected to LC-MS analysis.

Reaction mixtures (10 μL) containing 100 μM Mal-ACP, 25 μM AprA MT2, and 0.5 mM SAM, SAH, or sinefungin in 50 mM HEPES pH 7.4, 150 mM NaCl, 0.5 mM $MgCl_2$ were incubated at 30°C for 2 hr. Reactions were quenched with 10% (v/v) formic acid, and 0.2 μL of reaction mixtures were subjected to LC-MS analysis.

Reaction mixtures for intact protein analysis (10 μL) containing 100 μM AcAc-ACP, 25 μM AprA MT2, and 0.5 mM SAM in 50 mM HEPES pH 7.4, 150 mM NaCl, 0.5 mM $MgCl_2$ were incubated at 30°C for 15 min. Reaction mixtures for Ppant ejection analysis of amino acid variants (15 μL) containing 50 μM AcAc-ACP, 12.5 μM AprA MT2, and 0.5 mM SAM in 50 mM HEPES pH 7.4, 150 mM NaCl, 0.5 mM $MgCl_2$ were incubated at 30°C for 15 min. Reactions were quenched with 10% (v/v) formic acid, and 0.1 μL of reaction mixtures were subjected to LC-MS analysis.

Reactions (10 μL) to test AprA MT2 for acyltransfer activity contained 100 μM holo-ACP, 15 μM AprA MT2, 1 mM SAM, and 1 mM Mal-CoA in 50 mM HEPES pH 7.4, 150 mM NaCl were incubated at 30° C for 1 hr. Reactions were quenched with 10% (v/v) formic acid, and 0.1 μL of reaction mixtures were subjected to LC-MS analysis.

FabD Enzyme Assays

Reaction mixtures (120 μL) containing 100 μM AprA holo-ACP or AprI holo-ACP were incubated with 25 nM FabD and 0.85 mM Mal-CoA in 50 mM HEPES 7.4, 150 mM NaCl. Reactions were quenched (10 μL) with 10% (v/v) formic acid during a 10 min time course, and 1 μL of reaction mixtures were subjected to LC-MS analysis.

LC-MS Analysis

Assay reaction mixtures were analyzed using a simultaneous intact protein and phosphopantetheine (Ppant) ejection method[10, 11] on an Agilent Q-TOF 6545. Samples were subjected to reverse phase HPLC (Phenomenex Aeris widepore C4 column 3.6 μM, 50 x 2.10 mm) at a flow rate of 0.5 mL min^{-1} in H_2O with 0.2% (v/v) formic acid. Protein was eluted over 4 minutes with a gradient of 5-100% acetonitrile with 0.2% (v/v) formic acid. Reactions containing MT2 and AcAc-ACP and the FabD enzyme assays were subjected to the following conditions: fragmentor voltage, 300 V; skimmer voltage, 75 V; nozzle voltage, 1000 V; sheath gas temperature, 350 °C; drying gas temperature, 325 °C. In order to limit in-source decay of Mal-ACP, MeMal-ACP, and Me_2Mal-ACP, samples from corresponding reactions with AprA MT2 were analyzed using: fragmentor voltage, 225 V; skimmer voltage, 25 V; nozzle voltage, 1000 V; sheath gas temperature, 350 °C; drying gas temperature, 325 °C.

Data were processed using MassHunter Qualitative Analysis Software (Agilent). The maximum entropy deconvolution algorithm was used to obtain intact protein masses. The relative abundances of Ppant ejection fragments were used to calculate fractions of the ACP species. For FabD malonyl loading assays, the abundances of Mal-ACP and its in-source decay product acetyl-ACP were combined to calculate the amount of Mal-ACP produced.

HPLC Analysis

In order to analyze SAM consumption, 25 μL reaction mixtures containing 500 μM Mal-ACP, MeMal-ACP, or AcAc-ACP were incubated with 125 μM AprA MT2 and 0.5 mM SAM in 50 mM HEPES pH 7.4, 150 mM NaCl, 0.5 mM $MgCl_2$. Reactions were incubated for 10 min (MeMal-ACP), 15 min (AcAc-ACP), or 2 hr (Mal-ACP) at 30°C and quenched with 50 μL methanol. Precipitated protein was removed by centrifugation.

Reverse phase HPLC (Phenomenex Luna C18 column 5 μM, 250 x 4.6 mm) was used to separate small molecule components of the reaction (10 μL reaction mixtures, 2 μL of 1 mM SAM or 1 mM SAH standards) using HPLC buffer A (100 mM NaH_2PO_4, 75 mM NaOAc, pH 4.6) and HPLC buffer B (70% buffer A, 30% methanol) at a flow rate of 1 mL min^{-1}. Samples were injected onto the column equilibrated in 10% buffer B. Reaction components were eluted with a linear gradient to 30% buffer B (9% methanol) over 23 minutes. Absorbance was monitored at 254 nm.

Protein Crystallization and Structure Determination

AprA ΨGNAT-MT2 (503-1022) was crystallized by vapor diffusion in a 0.75:0.75 μL mixture of protein stock (5 mg mL^{-1} AprA in Tris buffer I with 1 mM SAM) and reservoir solution (0.01-0.05M trimethylamine *N*-oxide, 12-17% PEG 8000, 0.12 M Tris pH 7.5) in sitting drops at 20°C. Diffraction quality crystals obtained through micro seeding grew in 2-4 days. Crystals were cryoprotected with reservoir solution supplemented with 10% glycerol, and flash cooled in liquid N_2.

Diffraction data were collected at 100 K on GM/CA beamline 23ID-B at the Advanced Photon Source (APS) at Argonne National Laboratory (Argonne, IL). Data were processed using XDS[12].

The structure of AprA ΨGNAT-MT2 with bound SAH was solved by molecular replacement with Phaser[13] in the PHENIX software suite[14] using search models created with Sculptor[15] from the CurJ CMT (33% identity, PDB code: 5THY)[16] and CurA GNAT (24% identity, PDB code: 2REE)[17]. The initial model was modified with AutoBuild[18] to generate a 77% complete model of the AprA ΨGNAT-MT2. The remaining portion of the model was completed manually using Coot[19]. Refinement was performed using phenix.refine[20]. The structure was validated with MolProbity[21]. Figures were prepared using PyMOL[22]. Sequence alignments were prepared using Clustal[23] through Jalview[24]. The dendrogram was created using the average distance BLOSUM62 algorithm in Jalview.

Negative-stain electron microscopy

AprA ΔACP was prepared following a negative staining protocol[25] and imaged at 120 kV using a Tecnai T12 electron microscope (FEI). A total of 200 micrographs were taken at 52,000x nominal magnification using a 4k by 4k CCD camera (Gatan). Images were binned by 2 resulting in a sampling of 4.32 Å per pixel for particle picking and processing. ~50,000 particles were selected automatically, then subject to reference-free 2D classifications using RELION[26], resulting in ~15,000 particles corresponding to the "linear" state and ~15,000 particles corresponding to the "bent" state. The remaining particles were found in classes that corresponded to intermediate states or were in ambiguous orientations. Well-defined class average images in the bent state were selected to generate an initial model using e2initialmodel.py[27], and ~4,000 particles were extracted from the selected classes for 3D reconstruction. The initial model was filtered to 60-Å resolution, and then subjected to 3D auto-refinement with C2 symmetry enforced. The resulting model showed a resolution of ~26 Å (gold

standard FSC criterial of 0.143). Crystal structures of the MT1-ΨGNAT monomer and MT2 dimer were docked as rigid bodies into the EM density in Chimera[28], as an extensive interface exists between MT1 and ΨGNAT, whereas few contacts are observed between ΨGNAT and MT2. Additionally, MT1 is not soluble without ΨGNAT, while MT2 can be independently excised from AprA. Figures of the EM model were prepared using Chimera[28].

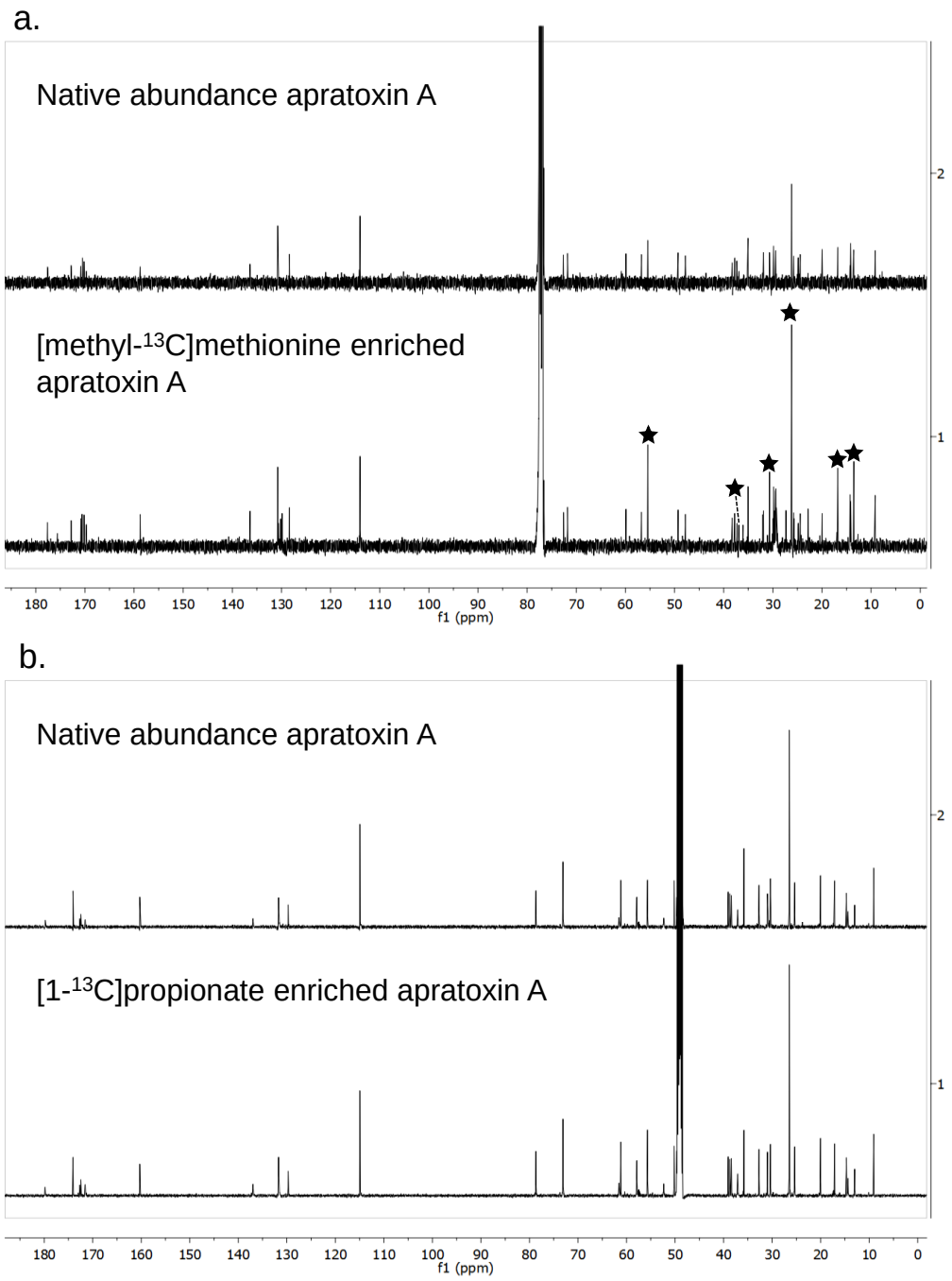

Figure S1: Comparison of ^{13}C-NMR enrichment with methionine and propionate. (**a**) Unlabeled apratoxin A on top compared with apratoxin A labeled with [methyl-^{13}C]methionine on bottom (in $CDCl_3$). Stars indicate enriched carbon resonances. (**b**) Unlabeled apratoxin A on top compared with apratoxin A labeled with [1-^{13}C]propionate on bottom (in D_4-MeOH). There is no significant enrichment in any of the ^{13}C resonances.

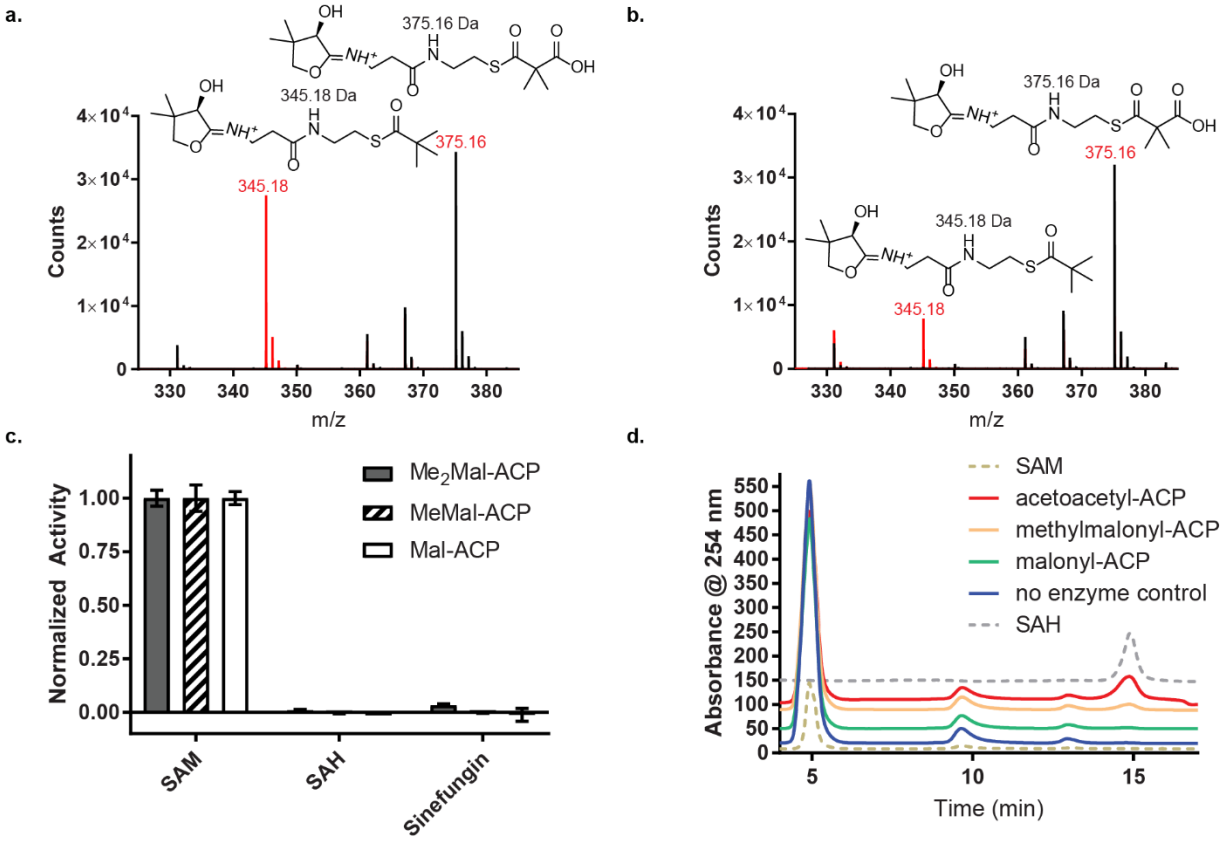

Figure S2: Assay data. Ppant ejection data for dimethylmalonyl-ACP (generated with AprA MT1) production by (**a**) AprA MT2 and (**b**) BryX MT2 in Figure 2a. Mass spectra from reactions are in red, no-enzyme negative controls in black. Experimentally observed masses are in red, calculated masses in black. (**c**) Relative activities for reactions of AprA MT2 with Me_2Mal-ACP, MeMal-ACP, Mal-ACP, in the presence of SAM, SAH, and sinefungin. Data represent total product formed. All reaction species were quantified using the Ppant ejection assay[10, 11]. Error bars, in some cases too small to be visible, represent triplicate experiments. (**d**) HPLC analysis of SAM consumption in reactions of AprA MT2 with Mal-ACP, MeMal-ACP and AcAc-ACP. SAM and SAH standards are shown in dashed lines.

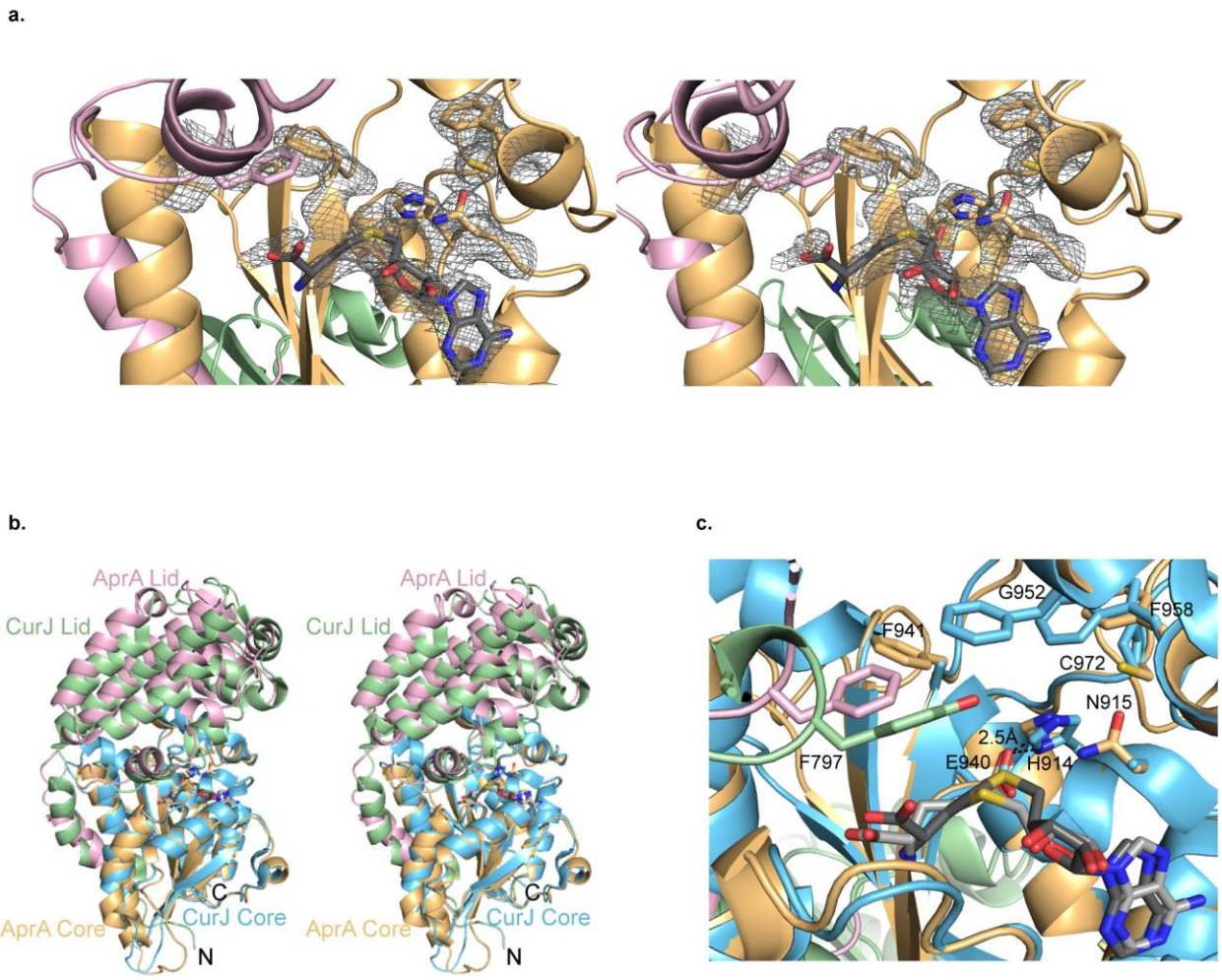

Figure S3: AprA MT2 omit density and comparison between AprA MT2 and CurJ *C*-MT. (**a**) 2Fo-Fc composite omit density around MT2 active site contoured at 1σ in stereo. Maps were calculated with simulated annealing (starting temperature 5000 K). (**b**) AprA MT2 (pink lid, orange core) and CurJ *C*-MT (green lid, blue core) superimposed by their core domains (RMSD of 0.48 Å for 103 Cα atoms). SAH is shown in sticks with atomic coloring (C, gray). Key active site residues are shown in sticks. (**c**) Zoom view of the AprA MT2 and CurJ *C*-MT active sites from the superposition in b. Labels correspond to mutagenized amino acids in AprA MT2.

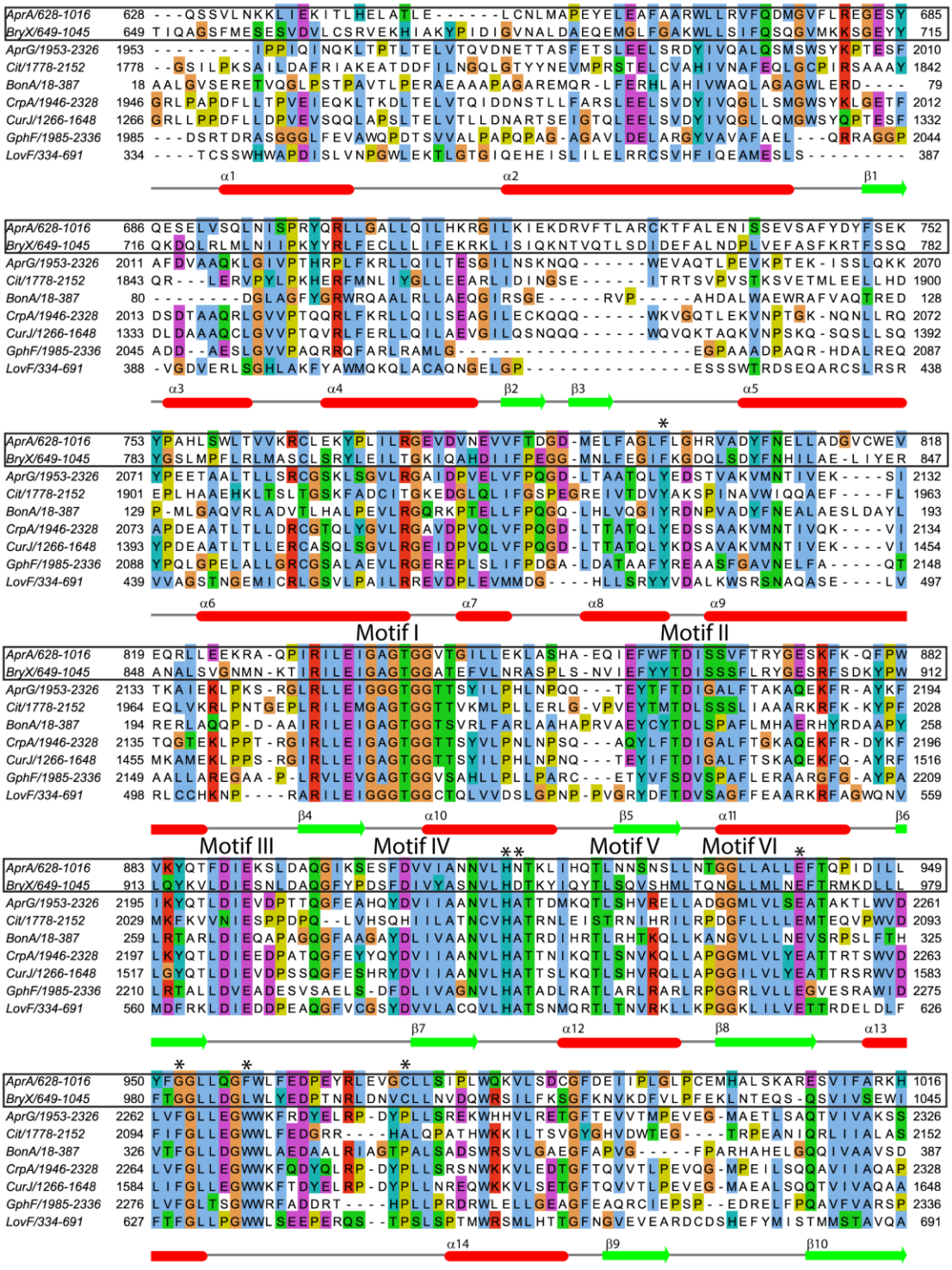

Figure S4: AprA MT2 sequence alignment and secondary structure with BryX MT2 and PKS *C*-MTs. AprA amino acids subjected to mutagenesis are starred and class I MT motifs are labeled. Abbreviations (GenBank accession codes): Apr, apratoxin A (WP_075900460); Bry, bryostatin (ABK51302.1); Cit, citrinin (A0A161CEU9.1); Crp, cryptophycin (ABM21569.1); Cur, curacin A (WP_008191795.1); Gph, gephyronic acid (AHA38199.1); Lov, lovastatin (Q9Y7D5.1).

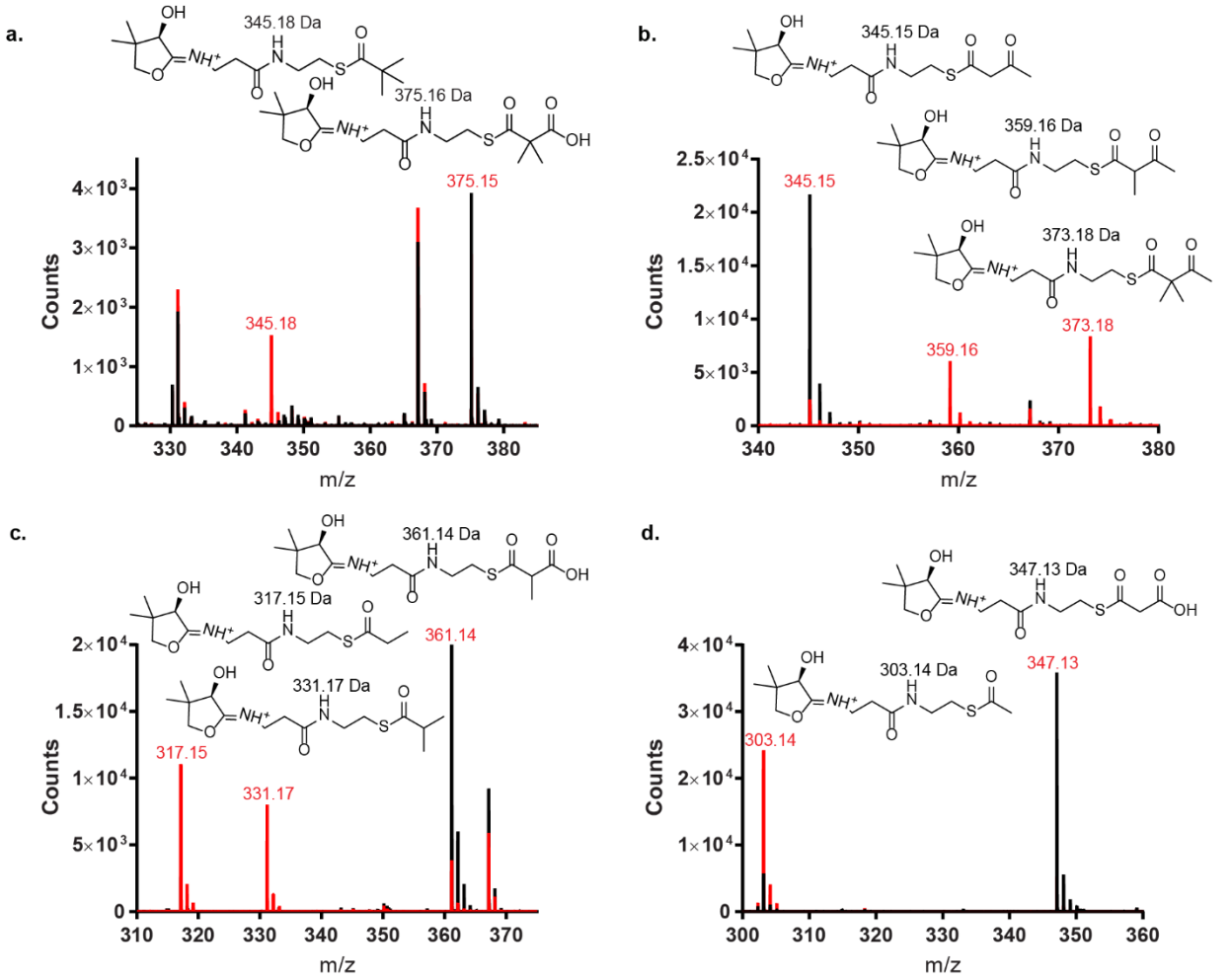

Figure S5: Representative Ppant ejection data for (**a**) Me_2Mal-ACP (generated with Me_2Mal-thiophenol) (**b**) AcAc-ACP, (**c**) MeMal-ACP and (**d**) Mal-ACP. Reactions with AprA MT2 are in red, no enzyme control in black. Experimentally observed masses are in red, calculated masses in black.

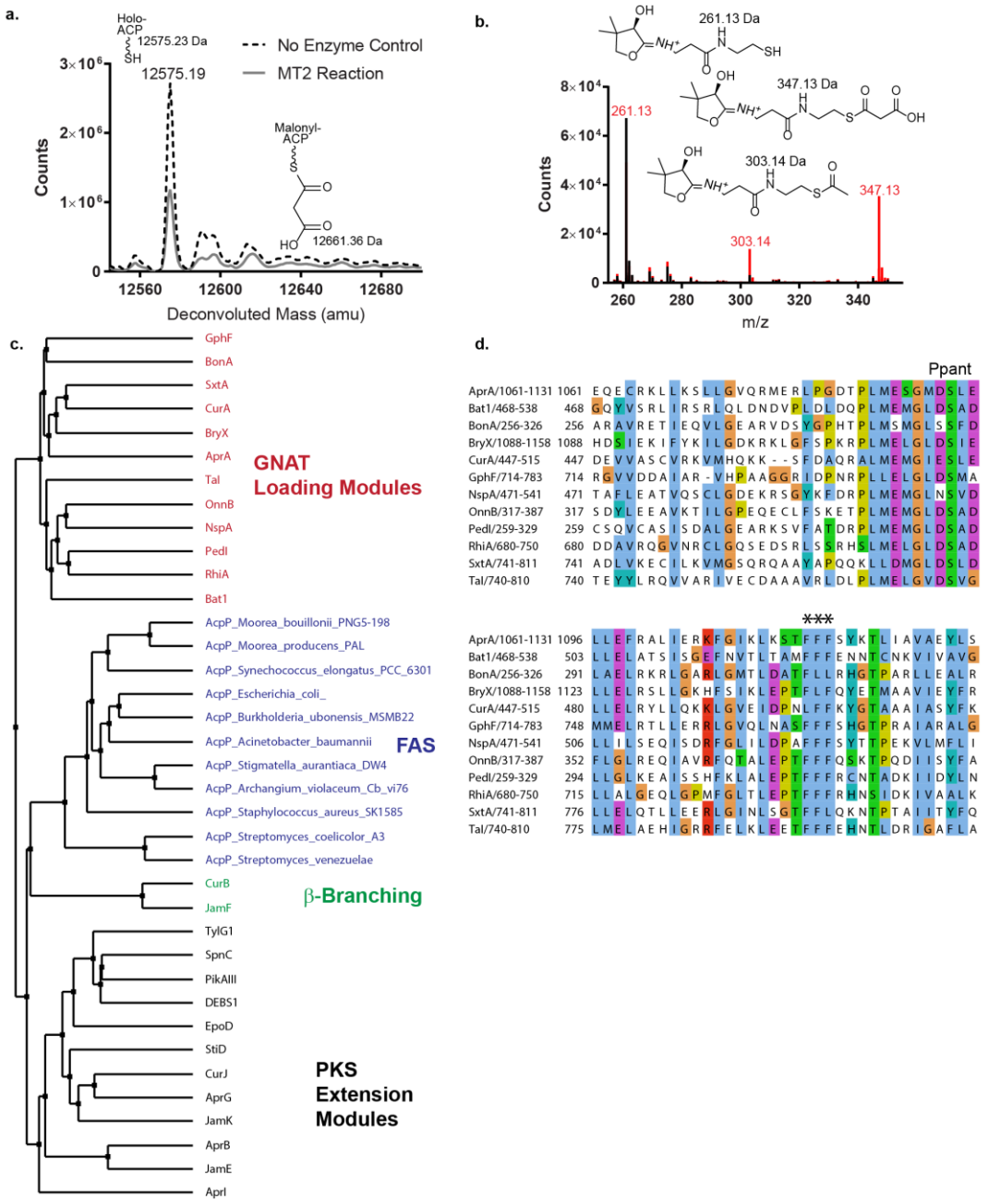

Figure S6: Acyltransfer activity and GNAT loading-module-associated ACPs. (**a**) Intact protein mass spectra of AprA ACP loading reactions of MT2 with Mal-CoA and holo-ACP. Calculated masses are indicated next to chemical structures, observed masses are indicated on spectra. No acyltransfer was observed in a 1 hr reaction. (**b**) Representative Ppant ejection data for reactions of FabD with Mal-CoA and AprA holo-ACP. Reaction with FabD is in red, no enzyme control in black. The presence of acetyl-ACP is due to in source decay during ionization.
(**c**) Dendrogram of ACPs from GNAT loading modules (red), fatty acid synthase AcpP (blue), PKS β-branching (green), PKS extension modules (black). (**d**) Sequence alignment of GNAT associated ACPs. Ppant attachment site (Ser1093) is labeled. Phenylalanine-containing motif specific to ACPs in GNAT loading modules is marked with asterisks. Pathway abbreviations

(GenBank accession codes) are as follows: Apr, apratoxin A (WP_075900460); Bry, bryostatin (ABK51302.1); Cur, curacin A (AEE88289.1); Sxt, saxitoxin (WP_009343302.1); Ta, myxovirescin A (WP_011553948.1); Gph, gephyronic acid (KF479198.1); Rhi, rhizoxin (WP_013435483.1); Nsp, nosperin (ADA69237.1); Bat, batumin (WP_052451043.1); Onn, onnamide (AAV97870.1); Ped, pederin (AAR19304.1); Bon, bongkrekic acid (AFN27480.1).

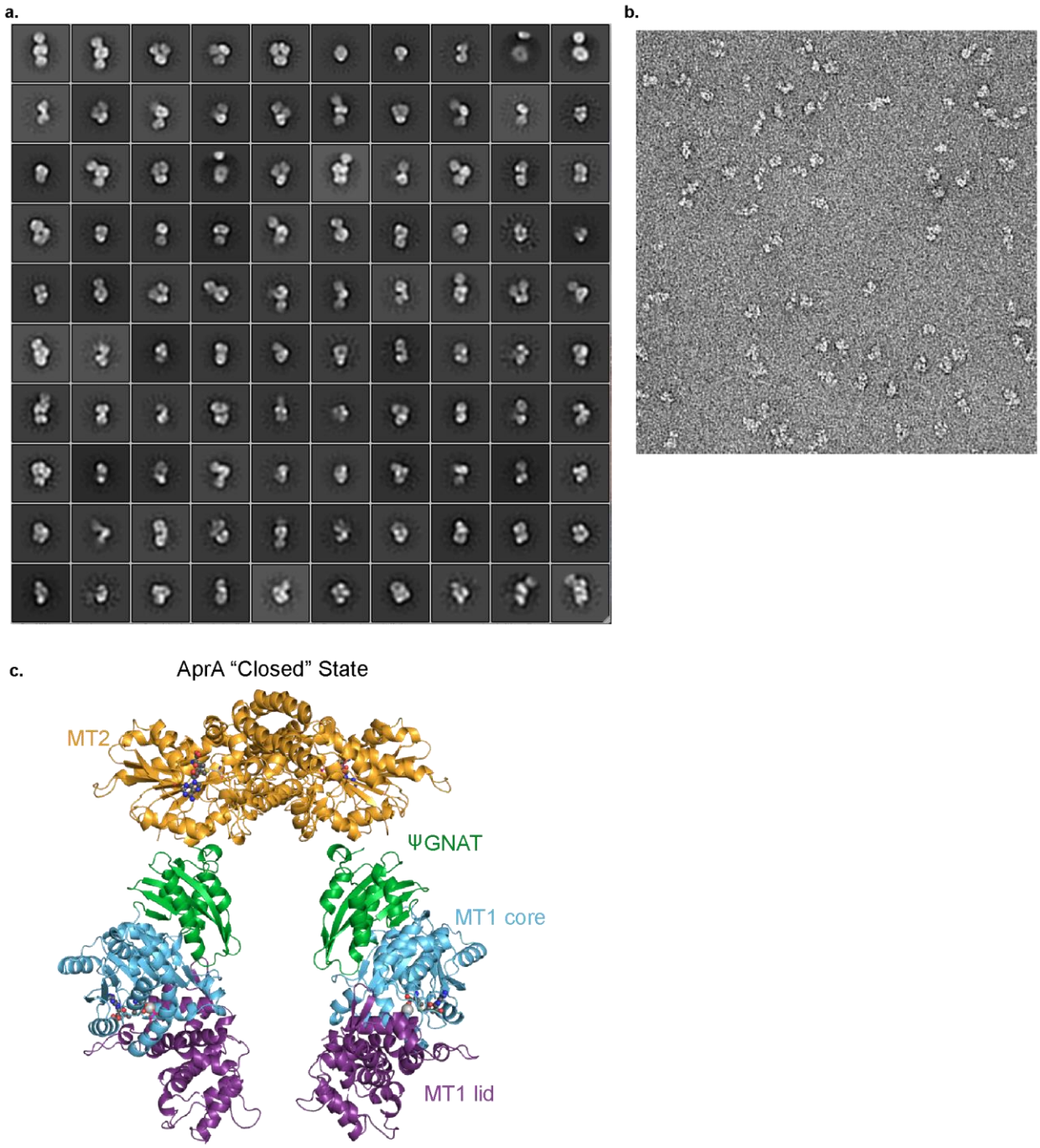

Figure S7: EM and AprA model. (**a**) Negative stain class averages of AprA ΔACP. (**b**) Raw negative stain micrograph of AprA ΔACP. (**c**) Model of AprA based on a 3D reconstruction of bent-state particles, colored as in Fig. 6. Compared to the linear-state model from superposition of the MT1-ΨGNAT and ΨGNAT-MT2 crystal structures, the MT1-ΨGNAT is rotated ~45° relative to the MT2 dimer.

Table S1: Enrichment of ^{13}C in apratoxin A by culture of *M. bouillonii* PNG 5-198 in media supplemented with [1-^{13}C]propionate. Final enrichment values are derived by normalization of enriched ^{13}C-NMR resonances to five different carbon atoms. Calculation steps are detailed in methods. C39 enrichment value is italicized and bolded in columns 21 and 22.

Column # →																					
1	2	3	4	5	6	7	8	9	10	11	12	13	14	15	16	17	18	19	20	21	22
	Biosynthetic		Integral of unlabeled	Normalization factor using:					Integral of enriched	Normalized integral of enriched sample using:					Enrichment compared to:					Average %	Fold
C#	source	ppm	resonance	C7	C13	C20	C30	C37	resonance	C7	C13	C20	C30	C37	C7	C13	C20	C30	C37	enrichment	change
1	Pro	174.1	45.5	0.5	0.9	0.9	0.2	0.3	56.0	44.5	63.0	50.2	50.6	52.1	25.8	-11.2	11.6	10.7	7.4	8.8	1.1
2	Pro	61.2	91.4	0.9	1.8	1.7	0.4	0.5	97.9	89.6	126.8	100.9	101.8	104.9	9.3	-22.8	-3.0	-3.8	-6.6	-5.4	0.9
3	Pro	29.8	2.2	0.0	0.0	0.0	0.0	0.0	2.9	2.1	3.0	2.4	2.4	2.5	37.2	-3.1	21.8	20.8	17.2	18.8	1.2
4	Pro	25.9	1.6	0.0	0.0	0.0	0.0	0.0	7.5	1.5	2.2	1.7	1.7	1.8	389.0	245.4	334.0	330.4	317.7		1.0
5[1]	Pro	N.P.	-	-	-	-	-	-	-	-	-	-	-	-	-	-	-	-	-	-	-
6	Ile	172.7	32.0	0.3	0.6	0.6	0.2	0.2	38.7	31.4	44.4	35.3	35.6	36.7	23.5	-12.8	9.6	8.7	5.5	6.9	1.1
7	Ile	57.9	97.8	1.0	1.9	1.8	0.5	0.6	95.8	95.8	135.6	107.9	108.8	112.1	0.0	-29.4	-11.3	-12.0	-14.6	-13.4	0.9
8	Ile	31.0	65.8	0.7	1.3	1.2	0.3	0.4	79.9	64.4	91.2	72.6	73.2	75.4	24.0	-12.4	10.1	9.2	5.9	7.4	1.1
9	Ile	25.3*	173.2	1.8	3.4	3.2	0.8	1.0	198.6	169.6	240.2	191.1	192.7	198.6	17.1	-17.3	3.9	3.0	0.0	1.3	1.0
10	Ile	9.1	79.2	0.8	1.6	1.5	0.4	0.5	91.9	77.6	109.9	87.4	88.2	90.8	18.5	-16.3	5.1	4.3	1.2	2.5	1.0
11	Ile	14.7	73.3	0.7	1.4	1.4	0.4	0.4	85.5	71.8	101.6	80.9	81.6	84.0	19.1	-15.9	5.7	4.8	1.7	3.1	1.0
12	SAM	30.4	93.6	1.0	1.8	1.8	0.5	0.5	91.5	91.7	129.8	103.3	104.2	107.4	-0.2	-29.6	-11.5	-12.2	-14.8	-13.7	0.9
13	Ala	171.6	51.0	0.5	1.0	1.0	0.2	0.3	70.7	50.0	70.7	56.3	56.8	58.5	41.6	0.0	25.7	24.6	20.9	22.6	1.2
14	Ala	61.6	58.7	0.6	1.2	1.1	0.3	0.3	71.3	57.5	81.4	64.8	65.3	67.3	24.0	-12.4	10.1	9.1	5.9	7.4	1.1
15	Ala	14.4	64.4	0.7	1.3	1.2	0.3	0.4	70.6	63.1	89.3	71.1	71.7	73.9	11.8	-21.0	-0.7	-1.6	-4.5	-3.2	1.0
16	SAM	35.8	82.8	0.8	1.6	1.6	0.4	0.5	86.3	81.1	114.8	91.4	92.2	95.0	6.5	-24.8	-5.5	-6.3	-9.1	-7.9	0.9
17	Tyr	172.4	43.3	0.4	0.8	0.8	0.2	0.3	51.2	42.4	60.1	47.8	48.2	49.7	20.6	-14.8	7.0	6.2	3.0	4.4	1.0
18	Tyr	52.3	61.2	0.6	1.2	1.1	0.3	0.4	84.0	60.0	84.9	67.6	68.1	70.2	40.1	-1.0	24.3	23.3	19.7	21.3	1.2
19	Tyr	37.1	130.5	1.3	2.6	2.4	0.6	0.8	155.9	127.8	181.0	144.0	145.2	149.6	22.0	-13.9	8.2	7.3	4.2	5.6	1.1
20	Tyr	129.7	53.3	0.5	1.0	1.0	0.3	0.3	58.9	52.2	74.0	58.9	59.4	61.2	12.7	-20.4	0.0	-0.8	-3.8	-2.5	1.0
21/25	Tyr	131.7	214.8	2.2	4.2	4.0	1.0	1.2	243.0	210.4	297.9	237.1	239.1	246.3	15.5	-18.4	2.5	1.6	-1.4	0.0	1.0
22/24	Tyr	115.0	206.4	2.1	4.0	3.9	1.0	1.2	215.3	202.1	286.2	227.8	229.7	236.7	6.5	-24.8	-5.5	-6.3	-9.0	-7.8	0.9
23	Tyr	160.3	50.0	0.5	1.0	0.9	0.2	0.3	48.6	48.9	69.3	55.2	55.6	57.3	-0.7	-29.9	-11.9	-12.7	-15.2	-14.1	0.9
26	SAM	55.7	100.0	1.0	2.0	1.9	0.5	0.6	100.0	97.9	138.7	110.4	111.3	114.7	2.1	-27.9	-9.4	-10.2	-12.8	-11.6	0.9
27	Acetate	171.3	4.8	0.0	0.1	0.1	0.0	0.0	4.6	4.7	6.6	5.3	5.3	5.5	-1.5	-30.5	-12.6	-13.4	-15.9	-14.8	0.9
28[2]	Acetate	N.P.	8.3	-	-	-	-	-	-	-	-	-	-	-	-	-	-	-	-	-	-
29	Cys	137.0	58.0	0.6	1.1	1.1	0.3	0.3	80.2	56.8	80.5	64.0	64.6	66.5	41.2	-0.3	25.3	24.2	20.6	22.2	1.2
30	Cys	73.1*	207.4	2.1	4.1	3.9	1.0	1.2	230.8	203.1	287.6	228.9	230.8	237.8	13.6	-19.7	0.8	0.0	-2.9	-1.6	1.0
31	Cys	38.4	76.2	0.8	1.5	1.4	0.4	0.4	94.2	74.7	105.7	84.1	84.9	87.4	26.2	-10.9	12.0	11.0	7.8	9.2	1.1
32	SAM	13.0	72.5	0.7	1.4	1.4	0.3	0.4	87.3	71.0	100.5	80.0	80.7	83.1	23.0	-13.1	9.2	8.3	5.1	6.5	1.1
33	Acetate	179.8	43.7	0.4	0.9	0.8	0.2	0.3	43.7	42.8	60.6	48.2	48.6	50.1	2.1	-27.9	-9.4	-10.2	-12.8	-11.6	0.9
34	Acetate	50.2	76.2	0.8	1.5	1.4	0.4	0.4	92.0	74.6	105.6	84.1	84.8	87.4	23.3	-12.9	9.4	8.5	5.3	6.7	1.1
35	Acetate	73.1*	207.4	2.1	4.1	3.9	1.0	1.2	230.8	203.1	287.6	228.9	230.8	237.8	13.6	-19.7	0.8	0.0	-2.9	-1.6	1.0
36	Acetate	39.1	79.8	0.8	1.6	1.5	0.4	0.5	94.7	78.2	110.7	88.1	88.8	91.5	21.1	-14.5	7.5	6.6	3.4	4.8	1.0
37	Acetate	25.3*	173.2	1.8	3.4	3.2	0.8	1.0	198.6	169.6	240.2	191.1	192.7	198.6	17.1	-17.3	3.9	3.0	0.0	1.3	1.0
38	Acetate	38.7	77.6	0.8	1.5	1.5	0.4	0.4	82.8	76.0	107.6	85.6	86.4	89.0	9.0	-23.0	-3.3	-4.1	-6.9	-5.7	0.9
39	Acetate	78.7	87.4	0.9	1.7	1.6	0.4	0.5	102.0	85.6	121.2	96.5	97.3	100.2	19.2	-15.9	5.7	4.9	1.8	***3.1***	***1.0***
40	Acetate	32.7	93.5	1.0	1.8	1.8	0.5	0.5	93.8	91.6	129.7	103.2	104.1	107.3	2.3	-27.7	-9.2	-9.9	-12.6	-11.4	0.9
41-43	SAM	26.5	404.2	4.1	7.9	7.6	1.9	2.3	487.6	395.8	560.5	446.1	449.8	463.5	23.2	-13.0	9.3	8.4	5.2	6.6	1.1
44	SAM	17.1	88.5	0.9	1.7	1.7	0.4	0.5	95.7	86.7	122.7	97.7	98.5	101.5	10.4	-22.0	-2.0	-2.8	-5.7	-4.4	1.0
45	Acetate	20.0	89.7	0.9	1.8	1.7	0.4	0.5	103.2	87.8	124.4	99.0	99.8	102.8	17.5	-17.0	4.2	3.4	0.3	1.7	1.0

*Overlapping ^{13}C-NMR shifts. The enrichment values cannot be distinguished, so both are reported.

[1]C5 – N.P. = No quantitation. C5 obscured by D_4-MeOH solvent peak.

[2]C28 – N.P. = No quantitation. Weak signal observed in native abundance, but not enriched sample.

Table S2: ^{13}C-NMR shifts of native-abundance apratoxin A in $CDCl_3$ and D_4-MeOH, [methyl-^{13}C]methionine labeled apratoxin A in $CDCl_3$, and [1-^{13}C]propionate-labeled apratoxin A in D_4-MeOH.

	[methyl-^{13}C] methionine labeled CDCl3	Native abundance $CDCl_3$	[1-^{13}C]propionate-labeled D_4-MeOH	Native abundance D_4-MeOH
C#	ppm	ppm	ppm	ppm
1	172.8	172.8	174.1	174.1
2	59.9	59.9	61.2	61.2
3	29.5	29.4	29.8	29.8
4	25.8	25.8	25.9	25.9
5	47.8	47.8	47.5	47.5
6	170.8	170.8	172.7	172.7
7	56.8	56.7	57.9	57.9
8	31.9	31.9	31.0	31.0
9	24.8	24.8	25.3	25.3
10	9.2	9.2	9.1	9.1
11	14.2	14.2	14.7	14.7
12	30.7	30.7	30.4	30.4
13	170.2	170.2	171.6	171.6
14	60.9	60.8	61.6	61.6
15	14.1	14.1	14.4	14.4
16	36.9	36.9	35.8	35.8
17	170.6	170.5	172.4	172.4
18	50.6	50.6	52.3	52.3
19	37.3	37.4	37.1	37.1
20	128.4	128.4	129.7	129.7
21/25	130.8	130.8	131.7	131.7
22/24	114.0	114.0	115.0	115.0
23	158.8	158.8	160.3	160.3
26	55.4	55.4	55.7	55.7
27	169.7	169.7	171.3	171.3
28	130.6	130.6	N.P.	130.8
29	136.4	136.4	137.0	137.0
30	72.6	72.6	73.1	73.1
31	37.7	37.7	38.4	38.4
32	13.5	13.5	13.0	13.0
33	177.6	177.6	179.8	179.8
34	49.3	49.3	50.2	50.2
35	71.8	71.8	73.1	73.1
36	38.3	38.3	39.1	39.1
37	24.4	24.4	25.3	25.3
38	37.8	37.8	38.7	38.7
39	N.P.*	N.P.	78.7	78.7
40	35.0	35.0	32.7	32.7
41/42/43	26.2	26.2	26.5	26.5
44	16.8	16.8	17.1	17.1
45	20.0	20.0	20.0	20.0

* N.P. indicates no peak observed. Overlapping resonances are italicized - shifts in D_4-MeOH confirmed by HSQC/HMBC (data not shown).

Table S3: Crystallographic data collection and refinement

Data Collection	
Space group	*C*2
Cell dimensions a,b,c (Å)	152.4, 54.2, 109.3
α,β,γ (°)	90, 131.8, 90
X-ray source	APS 23ID-B
Wavelength (Å)	1.0332
d_{min} (Å)	2.25 (2.38-2.25)[1]
R_{merge}	0.090 (0.998)
Wilson B factor	53.0
Avg I/σ(I)	10.87 (1.53)
Completeness (%)	98.4 (97.8)
Multiplicity	6.1 (6.4)
Total observations	191,196 (31,888)
$CC_{1/2}$	0.998 (0.720)
CC*	0.999 (0.915)
Refinement	
Data range (Å)	48.86-2.25
Reflections in refinement (#)	31,507
R_{work}/R_{free}	17.4/23.0
Non-hydrogen atoms (#)	4,317
protein	4,161
ligand	31
water	125
Amino acid residues	511
Deviation from ideality	
bond lengths (Å)	0.008
bond angles (°)	0.983
Average B-factor	68.1
macromolecule	68.3
ligand	96.2
solvent	62.2
Ramachandran plot	
favored (%)	95.9
allowed (%)	3.9
outliers (%)	0.2

[1] Values in parentheses pertain to outermost shell of data.

Table S4: Primer sequences.

AprA ΨGNAT-MT2 (502-1022)	pAPS4_F	**TACTTCCCATCCAATGCA**GAAAAGCGCAAATATCAGATACGGTATGCAACT
	pAPS4_R	**TTATCCACTTCCAATGTTA**TGTTTTCTCCTGTACTTGATGC
AprA ΔACP (2-1034)	pAPS5_F	**TACTTCCAATCCAATGCA**CTAGATAAAATAAATCGTTATGCTCATGGGTTTGTAGC
	pAPS5_R	**TTATCCACTTCCAATGTTA**ATTTTCTGTCAAATTTTGTTTAATTTTTTC
AprA MT2 (628-1022)	pMAS247_F	**TACTTCCAATCCAATGCGCA**ATCTTCAGTTTTAAACAAAAAGCTTATAG
	pMAS247_R	**TTATCCACTTCCAATGTTA**TGTTTTCTCCTGTACTTGATGC
FabD	pMAS337_F	**TACTTCCAATCCAATGCC**ATGATAAAGACTGCATGGGTGTTTCCCG
	pMAS337_R	**TTATCCACTTCCAATGCTA**CCTTACTACTAAGCATTGCTGCAGATCAG
AprI ACP (2085-2201)	pMAS373_F	**TACTTCCAATCCAATGCC**TCAATAGCTACAAAGGATAATCTCCTTTTAGAAC
	pMAS373_R	**TTATCCACTTCCAATGCTA**TAGCTCTACCTCTATCCAGTTATTTTCTTTAATG
BryX MT2 (656-1052)	pMAS308_F	**TACTTCCAATCCAATGCC**ATGGAAAGTGAGTCAGTTGATGTT
	pMAS308_R	**TTATCCACTTCCAATGCTA**ATTACTAGACAGGTCTTCATTAATCC
AprA MT2 F797Y	pMAS310_ F	GATATGGAGCTATTTGCTGGACTATATCTAGGACATCGT
	pMAS310_R	ACGATGTCCTAGATATAGTCCAGCAAATAGCTCCATATC
AprA MT2 H914N	pMAS260	ATGTGGTAATTGCTAATAACGTACTCAATAACACAAAATTAATTCATCAAACC
AprA MT2 N915A	pMAS252	GATGTGGTAATTGCTAATAACGTACTCCATGCCACAAAATTAATTCATCAAACCTTAAATAA
AprA MT2 E940A	pMAS312_ F	GGGGGTTATTGGCATTACTAGCGTTTACTCAACCAATTGATAT
	pMAS312_R	ATATCAATTGGTTGAGTAAACGCTAGTAATGCCAATAACCCCC
AprA MT2 G952F	pMAS311_ F	CTAGAGTTTACTCAACCAATTGATATTCTTTTATACTTTTTCGGGTTGCTTCAAGGATTTTG
	pMAS311_R	CAAAATCCTTGAAGCAACCCGAAAAAGTATAAAAGAATATCAATTGGTTGAGTAAACTCTAG
AprA MT2 F958W	pMAS381_ F	TACTTTGGAGGGTTGCTTCAAGGATGGTGGTTGTTTGAAGATCC
	pMAS381_R	GGATCTTCAAACAACCACCATCCTTGAAGCAACCCTCCAAAGTA
AprA MT2 C972P	pMAS315_ F	GAATACCGACTAGAAGTTGGTCCTTTACTGAGTATACCACTGTG
	pMAS315_R	CACAGTGGTATACTCAGTAAAGGACCAACTTCTAGTCGGTATTC
AprA MT2 C972S	pMAS319_ F	AATACCGACTAGAAGTTGGTAGTTTACTGAGTATACCACTG
	pMAS319_R	CAGTGGTATACTCAGTAAACTACCAACTTCTAGTCGGTATT

All sequences are 5'- 3'. Bold font indicates handles for ligation-independent insertion into expression vector.

Supporting References

[1] Chang, Z., Sitachitta, N., Rossi, J. V., Roberts, M. A., Flatt, P. M., Jia, J., Sherman, D. H., and Gerwick, W. H. (2004) Biosynthetic pathway and gene cluster analysis of curacin A, an antitubulin natural product from the tropical marine cyanobacterium *Lyngbya majuscula*, *J Nat Prod 67*, 1356-1367.

[2] Skiba, M. A., Sikkema, A. P., Moss, N. A., Tran, C. L., Sturgis, R. M., Gerwick, L., Gerwick, W. H., Sherman, D. H., and Smith, J. L. (2017) A mononuclear iron-dependent methyltransferase catalyzes initial steps in assembly of the apratoxin A polyketide starter unit, *ACS Chem Biol 12*, 3039-3048.

[3] Stols, L., Gu, M., Dieckman, L., Raffen, R., Collart, F. R., and Donnelly, M. I. (2002) A new vector for high-throughput, ligation-independent cloning encoding a tobacco etch virus protease cleavage site, *Protein Expr Purif 25*, 8-15.

[4] Sudek, S., Lopanik, N. B., Waggoner, L. E., Hildebrand, M., Anderson, C., Liu, H., Patel, A., Sherman, D. H., and Haygood, M. G. (2007) Identification of the putative bryostatin polyketide synthase gene cluster from "*Candidatus Endobugula sertula*", the uncultivated microbial symbiont of the marine bryozoan *Bugula neritina*, *J Nat Prod 70*, 67-74.

[5] Leao, T., Castelao, G., Korobeynikov, A., Monroe, E. A., Podell, S., Glukhov, E., Allen, E. E., Gerwick, W. H., and Gerwick, L. (2017) Comparative genomics uncovers the prolific and distinctive metabolic potential of the cyanobacterial genus *Moorea*, *Proc Natl Acad Sci U S A 114*, 3198-3203.

[6] Pfeifer, B. A., and Khosla, C. (2001) Biosynthesis of polyketides in heterologous hosts, *Microbiol Mol Biol Rev 65*, 106-118.

[7] Whicher, J. R., Smaga, S. S., Hansen, D. A., Brown, W. C., Gerwick, W. H., Sherman, D. H., and Smith, J. L. (2013) Cyanobacterial polyketide synthase docking domains: a tool for engineering natural product biosynthesis, *Chem Biol 20*, 1340-1351.

[8] Poust, S., Phelan, R. M., Deng, K., Katz, L., Petzold, C. J., and Keasling, J. D. (2015) Divergent mechanistic routes for the formation of gem-dimethyl groups in the biosynthesis of complex polyketides, *Angew Chem Int Ed Engl 54*, 2370-2373.

[9] Sánchez, C., Du, L., Edwards, D. J., Toney, M. D., and Shen, B. (2001) Cloning and characterization of a phosphopantetheinyl transferase from *Streptomyces verticillus* ATCC15003, the producer of the hybrid peptide-polyketide antitumor drug bleomycin, *Chem Biol 8*, 725-738.

[10] Meluzzi, D., Zheng, W. H., Hensler, M., Nizet, V., and Dorrestein, P. C. (2008) Top-down mass spectrometry on low-resolution instruments: characterization of

phosphopantetheinylated carrier domains in polyketide and non-ribosomal biosynthetic pathways, *Bioorg Med Chem Lett 18*, 3107-3111.

[11] Dorrestein, P. C., Bumpus, S. B., Calderone, C. T., Garneau-Tsodikova, S., Aron, Z. D., Straight, P. D., Kolter, R., Walsh, C. T., and Kelleher, N. L. (2006) Facile detection of acyl and peptidyl intermediates on thiotemplate carrier domains via phosphopantetheinyl elimination reactions during tandem mass spectrometry, *Biochemistry 45*, 12756-12766.

[12] Kabsch, W. (2010) Xds, *Acta Crystallogr D Biol Crystallogr 66*, 125-132.

[13] McCoy, A. J., Grosse-Kunstleve, R. W., Adams, P. D., Winn, M. D., Storoni, L. C., and Read, R. J. (2007) Phaser crystallographic software, *J Appl Crystallogr 40*, 658-674.

[14] Adams, P. D., Afonine, P. V., Bunkoczi, G., Chen, V. B., Davis, I. W., Echols, N., Headd, J. J., Hung, L. W., Kapral, G. J., Grosse-Kunstleve, R. W., McCoy, A. J., Moriarty, N. W., Oeffner, R., Read, R. J., Richardson, D. C., Richardson, J. S., Terwilliger, T. C., and Zwart, P. H. (2010) PHENIX: a comprehensive Python-based system for macromolecular structure solution, *Acta Crystallogr D Biol Crystallogr 66*, 213-221.

[15] Bunkoczi, G., and Read, R. J. (2011) Improvement of molecular-replacement models with Sculptor, *Acta Crystallogr D Biol Crystallogr 67*, 303-312.

[16] Skiba, M. A., Sikkema, A. P., Fiers, W. D., Gerwick, W. H., Sherman, D. H., Aldrich, C. C., and Smith, J. L. (2016) Domain organization and active site architecture of a polyketide synthase *C*-methyltransferase, *ACS Chem Biol 11*, 3319-3327.

[17] Gu, L., Geders, T. W., Wang, B., Gerwick, W. H., Hakansson, K., Smith, J. L., and Sherman, D. H. (2007) GNAT-like strategy for polyketide chain initiation, *Science 318*, 970-974.

[18] Terwilliger, T. C., Grosse-Kunstleve, R. W., Afonine, P. V., Moriarty, N. W., Zwart, P. H., Hung, L. W., Read, R. J., and Adams, P. D. (2008) Iterative model building, structure refinement and density modification with the PHENIX AutoBuild wizard, *Acta Crystallogr D Biol Crystallogr 64*, 61-69.

[19] Emsley, P., and Cowtan, K. (2004) Coot: model-building tools for molecular graphics, *Acta Crystallogr D Biol Crystallogr 60*, 2126-2132.

[20] Afonine, P. V., Grosse-Kunstleve, R. W., Echols, N., Headd, J. J., Moriarty, N. W., Mustyakimov, M., Terwilliger, T. C., Urzhumtsev, A., Zwart, P. H., and Adams, P. D. (2012) Towards automated crystallographic structure refinement with phenix.refine, *Acta Crystallogr D Biol Crystallogr 68*, 352-367.

[21] Chen, V. B., Arendall, W. B., 3rd, Headd, J. J., Keedy, D. A., Immormino, R. M., Kapral, G. J., Murray, L. W., Richardson, J. S., and Richardson, D. C. (2010) MolProbity: all-atom structure validation for macromolecular crystallography, *Acta Crystallogr D Biol Crystallogr 66*, 12-21.

[22] Schrodinger, LLC. (2015) The PyMOL Molecular Graphics System, Version 1.8.

[23] Larkin, M. A., Blackshields, G., Brown, N. P., Chenna, R., McGettigan, P. A., McWilliam, H., Valentin, F., Wallace, I. M., Wilm, A., Lopez, R., Thompson, J. D., Gibson, T. J., and Higgins, D. G. (2007) Clustal W and Clustal X version 2.0, *Bioinformatics 23*, 2947-2948.

[24] Waterhouse, A. M., Procter, J. B., Martin, D. M., Clamp, M., and Barton, G. J. (2009) Jalview Version 2--a multiple sequence alignment editor and analysis workbench, *Bioinformatics 25*, 1189-1191.

[25] Ohi, M., Li, Y., Cheng, Y., and Walz, T. (2004) Negative staining and image classification - powerful tools in modern electron microscopy, *Biol Proced Online 6*, 23-34.

[26] Scheres, S. H. (2012) RELION: implementation of a Bayesian approach to cryo-EM structure determination, *J Struct Biol 180*, 519-530.

[27] Tang, G., Peng, L., Baldwin, P. R., Mann, D. S., Jiang, W., Rees, I., and Ludtke, S. J. (2007) EMAN2: an extensible image processing suite for electron microscopy, *J Struct Biol 157*, 38-46.

[28] Pettersen, E. F., Goddard, T. D., Huang, C. C., Couch, G. S., Greenblatt, D. M., Meng, E. C., and Ferrin, T. E. (2004) UCSF Chimera--a visualization system for exploratory research and analysis, *J Comput Chem 25*, 1605-1612.